

SPHERE system analysis predictions

K. Dohlen^{1a}, F. Wildi², J.L. Beuzit³, P. Puget³, D. Mouillet³, A. Baruffolo⁴, A. Boccaletti⁵, J. Charton³, R. Claudi⁴, A. Costille³, P. Feautrier³, M. Feldt⁶, T. Fusco⁷, R. Gratton⁴, M. Kasper⁸, M. Langlois⁹, D. Le Mignant¹, J.L. Lizon⁸, N. Hubin⁸, A. Pavlov⁸, C. Petit⁷, J. Pragt¹⁰, P. Rabou³, S. Rochat³, R. Roelfsema¹⁰, J.F. Sauvage⁷, H.M Schmid¹¹

¹Laboratoire d'Astrophysique de Marseille - LAM, Université d'Aix-Marseille & CNRS, UMR7326, 38 rue F. Joliot-Curie, 13388 Marseille Cedex 13, France

²Observatoire de Genève, CH-1290 Sauverny, Switzerland

³Laboratoire d'Astrophysique de Grenoble, B.P. 53, F-38041 Grenoble Cedex 9, France

⁴Osservatorio Astronomico di Padova, Vicolo dell'Osservatorio 5, I-35122 Padova, Italy

⁵Laboratoire d'Etudes Spatiales et d'Instrumentation en Astrophysique, F-92190 Meudon, France

⁶Max Planck Institut für Astronomie, Königstuhl 17, D-69117 Heidelberg, Germany

⁷Office National d'Etudes et de Recherches Aérospatiales, B.P. 72, F-92322 Chatillon, France

⁸European Southern Observatory, Karl-Schwarzschild-Strasse 2, D-85748 Garching, Germany

⁹Laboratoire d'Astrophysique de Marseille, B.P. 8, F-13376 Marseille Cedex 12, France, now at CRAL

¹⁰ASTRON, P.O. Box 2, NL-7990 AA Dwingeloo, The Netherlands

¹¹Institute of Astronomy, ETH Zurich, CH-8092 Zurich, Switzerland

Abstract. SPHERE is an extra-solar planet imager instrument for ESO's VLT telescope. Scheduled for first light in 2012, aims to detect giant extra-solar planet in the vicinity of bright stars and to characterise the objects found through spectroscopic and polarimetric observations. The observations will be done both within the Y, J, H and Ks atmospheric windows ($\sim 0.95 - 2.32\mu\text{m}$) by the aid of a dual imaging camera (IRDIS) and an integral field spectrograph (IFS), and in the visible using a fast-modulating polarizing camera (ZIMPOL). The instrument employs an extreme-AO turbulence compensation system, focal plane tip-tilt correction, and interferential coronagraphs. The aim of this paper is to analyse the approach taken for system analysis and implementation in the light of forthcoming instruments of this type to be design and built for ELT-class telescopes.

1. Introduction

The SPHERE (Spectro-Polarimetric High-contrast Exoplanet Research) instrument [1,2] is built by a wide consortium of European countries. It is based on an extreme AO system (SAXO) [3] and employs coronagraphic devices [4] for stellar diffraction suppression. It is equipped with three science channels: a differential imaging camera (IRDIS) [5], an integral field spectrograph (IFS) [6], and a rapid switching polarimeter (ZIMPOL)[7], see Figure 1. In

^a e-mail: kjetil.dohlens@am.fr

Adaptive Optics for Extremely Large Telescopes II

this paper we present some of the essential elements of our approach to system analysis and performance prediction for the instrument.

Coming to completion ten years after first light of the previous generation AO systems such as NACO on the VLT, SPHERE differs from these systems in many ways. Of course, its adaptive optics module contains an order of magnitude more channels in its deformable mirror, allowing it not only to reach unprecedented Strehl ratios but also the high contrast levels required for exo-planet detection. But where previous-generation instruments were versatile, multi-purpose machines, SPHERE is a highly specialised instrument dedicated to high-contrast coronagraphy. While it still contains lots of stuff and supports a large number of observing and calibration modes, all the added features, from pupil stabilization and differential tip-tilt control to derotator optics and polarimetric components, are there for a single astronomical purpose. And there is none of the “nice to have” features that classical AO would be tempted to include, such as field selectors and general purpose IR WFS. SPHERE will certainly find uses beyond its single-minded objective, in particular filling the gap of high-resolution imaging in the visible in an era where the HST will have been decommissioned, but such users will have to accept the rules imposed by the instrument: highly performing, but strictly single conjugate adaptive optics.

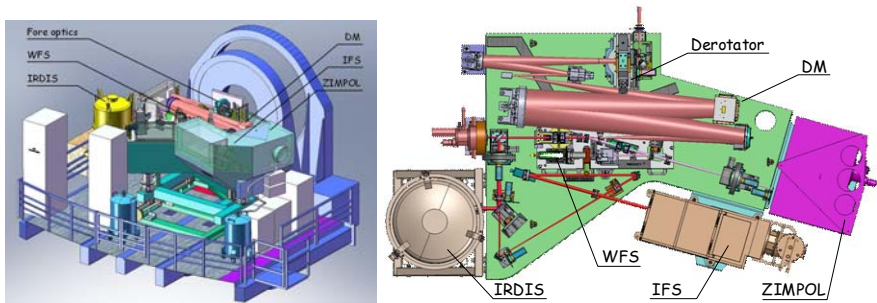


Fig. 1. Overview of the SPHERE instrument as installed on the Nasmyth platform of the VLT UT3 telescope. Key elements of the common optics system are indicated as well as the three science instruments: IRDIS, a near-infrared differential imaging camera and long slit spectrograph, IFS, a near-infrared integral-field spectrograph, and ZIMPOL, a visible imaging polarimeter.

The instrument suite includes a dual imaging camera (IRDIS), recording simultaneously two images at two close wavelengths. Assuming a sharp feature in the planetary spectrum, see Figure 2, it is therefore possible to distinguish between the speckle pattern (which has nearly the same contribution at the two wavelengths) and the faint planet. This basic technique, referred to as spectral difference imaging, will be completed by further image analysis techniques such as reference subtraction, angular differential imaging (ADI) [8].

The second focal plane instrument is an IFS working from $0.95 \mu\text{m}$ to $1.7 \mu\text{m}$ and providing low spectral resolution ($R \sim 30$) over a limited, $3'' \times 3''$, field of view. Data cubes produced by this instrument will be analysed using spectral deconvolution techniques [9], augmented with ADI analysis techniques.

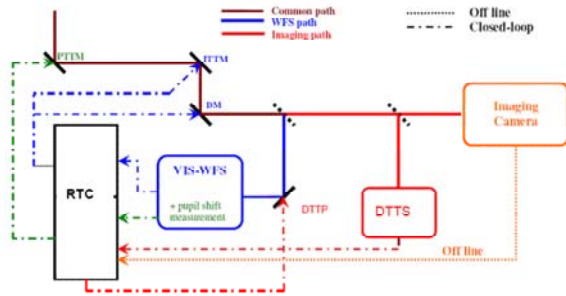


Fig. 5. Schematic drawing of the SPHERE adaptive optics system. Full lines indicate the light path, brown for common path, red for the IR path, and blue for the visible WFS path.

2. System analysis approach

2.1. Performance analysis concept

SPHERE performance analysis is built around two principal axes: image simulation based on the CAOS [10] environment, and an analytical approach linking imaging performance to the optical power spectral density function. This complementary approach allows on the one hand to predict with good precision the expected imaging quality by simulations, on the other hand to understand the origin of image degradations and to indicate laws of influence of various limiting factors. Both approaches link image quality to optical quality, requiring the implementation of an error budget in terms of power spectral density (PSD).

2.2. Power spectral density error budget

The PSF of an optical system is the magnitude square of the Fourier transform of the entrance pupil. It therefore contains two main components, the diffraction due to the pupil edges, corresponding to the Airy pattern, and the diffraction due to the phase aberrations in the system. Developing the mathematical expression of these terms leads to a combination of three terms: the Airy pattern, the PSD of the aberrations, and a cross term giving rise to “pinned speckles”, speckles located at the Airy rings. It can be seen that a good coronagraphic system, whose main role is to eliminate the Airy pattern, also eliminates or strongly reduces the level of pinned speckles. Estimating the PSD of the instrument is therefore of utmost importance.

PSD can be expressed in different ways, depending upon units and whether 1D or 2D measurements are used. We consider here the 2D version, and assume wavefront aberrations measured in nm and pupil dimensions in unit of pupil diameter. The unit of spatial frequency is then “cycles per pupil diameter” denoted by the unit c , and the PSD unit is nm^2 , signifying “nm squared per pupil cycle squared.” The advantage of using this unit instead of the more conventional nm^4 or nm^2mm^2 , signifying “nm squared per inverse mm squared,” is that individual surface PSD can be compared directly, whatever the size of the pupil on the surface. In particular, the PSD of the VLT primary mirror can be compared directly with the PSD of an internal surface a few mm across. Calculating the azimuthal average of the 2D PSD allows a convenient one-dimensional representation of this function.

Strictly speaking, computing the total instrument PSD would involve summing all the phase maps of the instrument before performing the Fourier transform. It is easily shown, however, that for isotropic surfaces and as long as we are interested in azimuthal statistics rather than exact distribution of speckle intensity, the cross-term is of no consequence and we can simply sum the individual surface PSDs.

Church [11] defines optical surface quality in terms of fractal finish, defining three different classes according to their spatial frequency power law: extreme (f^{-2}), Brownian (f^{-3}), and marginal (f^{-4}) fractal. In the search for typical PSDs valid for high-quality optical surfaces, we find that the current state of the art of optical polish, developed for UV lithography of electronic integrated circuits and reaching surface figure errors of 0.2nm RMS [12], generate extreme fractal surfaces, as can be seen in Figure 6. Such polish quality is achieved at the price of an exceedingly costly process, however, and For SPHERE we have therefore invested in high-quality classical polishing, achieving typically 1-2nm RMS surface figure. Again, typical PSDs that we have measured follow the same f^{-2} law indicating extreme fractal surfaces, see Figure 7. Based on these results, we take the assumption of extreme fractal for all our surfaces.

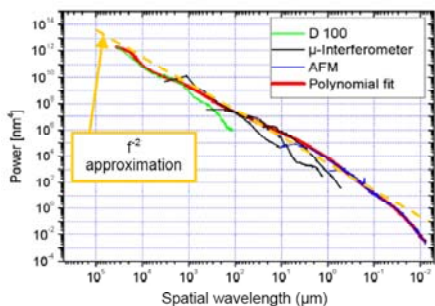


Fig. 6. Measured PSD of surfaces for UV lithography measured over several decades of spatial frequencies by different measurement apparatus. The orange broken line indicates the extreme fractal surface class. Adapted from [12].

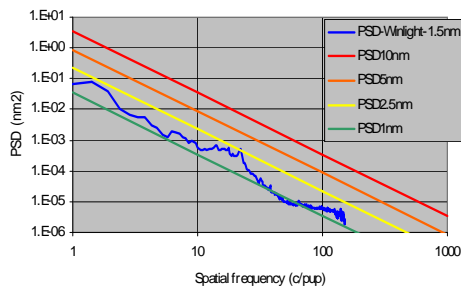


Fig. 7. Measured PSD of one of our prototype mirror surfaces (blue) compared with f^2 PSD representing 1nm (green) to 10nm (red) surfaces.

Further complexity of the PSD error budget is added by taking account of AO correction of aberrations below the AO cut-off frequency ($20c$ for a 40×40 actuator system) for optical surfaces upstream of the dichroic beam splitter, and correction of non-common path aberrations (NCPA) up to an estimated limit of $4c$ (approximately 50 Zernike terms) thanks to Phase Diversity [13] for surfaces downstream of the dichroic beam splitter, except the ADC which is rotating during observations.

In order to account for effects related to the presence of out-of-pupil surfaces, we have also included effects such as beam shift and Fresnel propagation.

2.3. Out-of-pupil aberrations: Beam shift

Beam shift occurs due to atmospheric dispersion, causing the visible beam observed by the WFS to pass through optical surfaces at a slightly different location than the infrared science

beam, inducing an error in the AO correction. An illustration of this effect is shown in Figure 8. For spatial frequencies $f \ll \delta p/d$, where δp is the induced shift and d is the local beam diameter, the PSD of the difference wavefront along the direction of the shift is approximately:

$$\Delta PSD = \left(\frac{2\pi f \delta p}{d} \right)^2 PSD$$

For our f^2 model, the result is a constant. Clearly, such beam shift phase maps are not isotropic, but we simplify the budget conservatively by assuming a rotationally symmetric PSD.

The effect has a noticeable impact on the PSD budget for some of the surfaces close to intermediate focal planes, such as the derotator mirrors. Quantitative assumptions of surface quality for these mirrors has allowed fixing lower limits to their out-of-image distances during the design phase of the instrument.

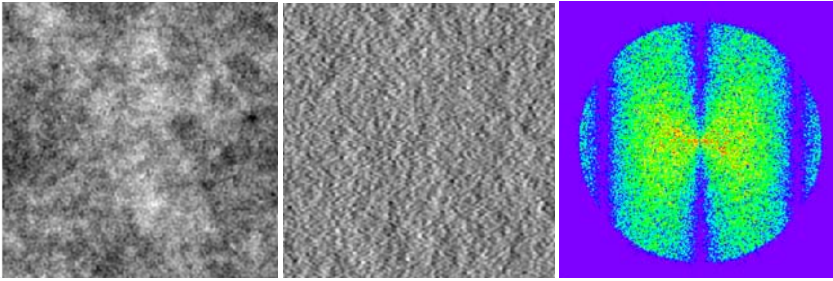


Fig. 8. Illustration of beam shift effects. Left: the original phase map of a f^2 PSD surface. Middle: The difference phase map corresponding to a small beam shift. Right: the PSD of the difference phase map.

2.4. The Fresnel-Talbot effect

The importance of Fresnel propagation of out-of pupil aberrations was underlined by Marois et al [14]. They described such propagation, where phase aberrations become transformed into intensity variations after a certain distance, in terms of the Talbot effect. Since the rate of transformation depends upon wavelength, the impact upon spectral differential imaging can be important.

We note that when associated with an optimal coronagraph, the effect of an out-of-pupil phase screen alone is of no consequence, indicating that the effect is less consequential in SPHERE than in the non-coronagraphic case considered. Still, when both in-pupil and out-of-pupil aberrations exist simultaneously, as they of course will do, cross terms appear. We find that the following expression represents the intensity of the spectral differential image in the presence of Fresnel propagation:

$$I_{SD}^F = I_{SD} + \sqrt{I_{Raw} I_{OutPup}} \sin(\pi \Delta N_T)$$

Adaptive Optics for Extremely Large Telescopes II

where I_{SD} is the intensity without the Fresnel effect, I_{Raw} is the intensity before spectral subtraction, I_{OutPup} is the intensity observed if the out-of-pupil aberration screen was the only aberration of the system, and $\Delta N_T = h/L_T \Delta\lambda/\lambda$ is the differential Talbot order, h is the propagation distance, $\Delta\lambda/\lambda$ is the fractional wavelength separation of the observed spectral bands, L_T is the Talbot length, $L_T = 2(D/f)^2/l$, D is the telescope pupil diameter, and f is the spatial frequency of the aberration. The “bulge” in the intensity profile predicted by this model has been confirmed by simulations, as shown in Figure 9. Again, the knowledge of this effect has guided the design of the instrument in terms of optical design and surface polish quality.

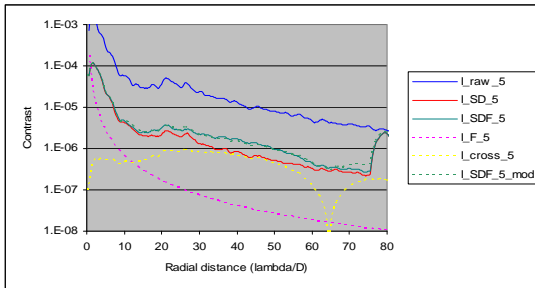


Fig. 9. The effect of Fresnel propagation in a spectral differential imaging system equipped with an ideal coronagraph. The bulge predicted by the model (yellow and green dotted lines) is reproduced with surprising accuracy by simulations (green solid line). The example concerns a 5nm RMS wavefront error introduced at a surface conjugated to a height of 420km above the telescope.

2.5. Expected performance

Based on the analysis indicated above, a PSD budget has been elaborated, see Figure 10. This PSD function is implemented into image simulation software, together with several other issues such as image centering and stability, realistic coronagraph devices, etc, in order to obtain an estimate of the final, post analysis contrast performance, see Figure 11.

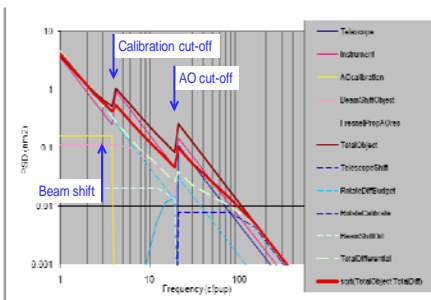


Fig. 10. PSD-based error budget for SPHERE taking into account assumed optical quality of all optical surfaces and estimated effects of several instrumental features such as beam-shift due to atmospheric dispersion, adaptive optics filtering and non-common-path aberration calibrations.

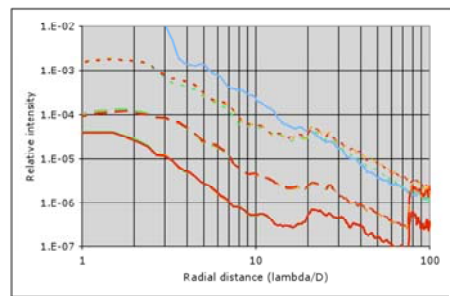


Fig. 11. Estimated contrast performance, showing five-sigma azimuthal statistics of the raw coronagraphic image (dotted line), of the spectral differential image (broken line), and of the reference subtraction (full line), compared with the azimuthally averaged non-coronagraphic image (blue).

3. Conclusions

After a brief description of the SPHERE instrument features, we describe the WFE budget elaborated in terms of PSD. The budget accounts for numerous instrumental effects such as beam shift etc. The budget feeds into performance simulations, providing estimated instrument performance in terms of five-sigma contrast levels. Predicted performance after spectral differencing and reference subtraction is compatible with goal specs, 10^{-5} at $0.1''$ and $5 \cdot 10^{-7}$ at $0.5''$

4. Acknowledgements

SPHERE is an instrument designed and built by a consortium of French, German, Italian, Swiss and Dutch institutes in collaboration with ESO. This paper is dedicated to the large group of people all across Europe who have been working since several years on all aspects of the instrument.

5. References

- [1] J.-L. Beuzit et al., *The Messenger* **125**, 29–34 (2006).
- [2] K. Dohlen, J.-L. Beuzit, M. Feldt et al., in: *Ground-based and Airborne Instrumentation for Astronomy*. Ed. McLean, Ian S.; Iye, Masanori. SPIE **6269**, pp. 62-69 (2006).
- [3] T. Fusco, C. Petit, J.-F. Sauvage et al., in *Advances in Adaptive Optics II*, Ed. Brent L. Ellerbroek, Domenico Bonaccini, SPIE **6272** (2006).
- [4] Anthony Boccaletti, Lyu Abe, Jacques Baudrand, et al., SPIE **7015** (2008).
- [5] K. Dohlen, M. Langlois, C. Moutou, et al., *Proc. SPIE* **7014** (2008).
- [6] R.U. Claudi, M. Turatto, J. Antichi, R. Gratton, et al., in: *Ground-based and Airborne Instrumentation for Astronomy*, Ed. Ian S. McLean, Masanori Iye, SPIE **6269** (2006).
- [7] Schmid, H. M.; Beuzit, J. L.; Mouillet, D. et al., in : *In the Spirit of Lyot 2010*, Ed. A. Boccaletti (2010).
- [8] C. Marois, D. Lafreniere, R. Doyon, B. Macintosh, D. Nadeau, *ApJ* **641**, 1, pp. 556-564 (2006).
- [9] N. Thatte, R. Abuter, M. Tecza, E.L. Nielsen, F.J. Clarke, L.M. Close, *MNRAS* **378**, 4, pp. 1229-1236 (2007).
- [10] M. Carillet, A. Boccaletti, C Thalmann, et al. SPIE **7017** (2008)
- [11] E. L. Church, *Appl. Opt.* **27**, 8, pp. 1518 (1988)
- [12] H. Enkisch, J. Trenkler, *Europhysics News* **35**, 5 (2004)
- [13] A. Blanc, T. Fusco, M. Hartung, L. M. Mugnier, and G. Rousset, *A&A* **399**, pp.373 (2003)
- [14] C. Marois, D. W. Phillion, B. Macintosh, in *Ground-based and Airborne Instrumentation for Astronomy*, ed. I. S. McLean, M. Iye, SPIE **6269**, 62693M (2006)